

Experiment study of energy redistribution during collisions of the excited state $H_2(1, 7)$ with LiH

Kai Wang(王凯), Zhong Liu(刘中), Shuying Wang(王淑英), Chu Qin(秦楚), Zilei Yu(於子雷), and Xiaofang Zhao(赵小芳)

Citation: Chin. Phys. B, 2025, 34 (**11**): 113401. DOI: 10.1088/1674-1056/add502
http://cpb.iphy.ac.cn; http://iopscience.iop.org/cpb

What follows is a list of articles you may be interested in

Theoretical investigations of population trapping phenomena in atomic four-color, three-step photoionization scheme

Xiao-Yong Lu(卢肖勇) and Ya-Peng Sun(孙亚鹏)
Chin. Phys. B, 2024, 33 (**3**): 033202. DOI: 10.1088/1674-1056/ad10fc

Light-shift induced by two unbalanced spontaneous decay rates in EIT (CPT) spectroscopies under Ramsey pulse excitation

Xiaoyan Liu(刘晓艳), Xu Zhao(赵旭), Jianfang Sun(孙剑芳), Zhen Xu(徐震), and Zhengfeng Hu(胡正峰)
Chin. Phys. B, 2021, 30 (**8**): 083203. DOI: 10.1088/1674-1056/ac0528

Quantal studies of sodium 3p←3s photoabsorption spectra perturbed by ground lithium atoms

N Lamoudi, F Talbi, M T Bouazza, M Bouledroua, K Alioua
Chin. Phys. B, 2019, 28 (**6**): 063202. DOI: 10.1088/1674-1056/28/6/063202

The ac Stark shifts of the terahertz clock transitions of barium

Yu Geng-Hua (余庚华), Geng Ying-Ge (耿鹰鸽), Li Long (李隆), Zhou Chao (周超), Duan Cheng-Bo (段丞博), Chai Rui-Peng (柴瑞鹏), Yang Yong-Ming (杨永明)
Chin. Phys. B, 2015, 24 (**10**): 103201. DOI: 10.1088/1674-1056/24/10/103201

Theoretical study of amplified spontaneous emission intensity and bandwidth reduction in polymer

A. Hariri, S. Sarikhani
Chin. Phys. B, 2015, 24 (**4**): 043201. DOI: 10.1088/1674-1056/24/4/043201

Experiment study of energy redistribution during collisions of the excited state $H_2(1, 7)$ with LiH

Kai Wang(王凯)[1,2,†], Zhong Liu(刘中)[1,2,†], Shuying Wang(王淑英)[1,2,‡], Chu Qin(秦楚)[1,2], Zilei Yu(於子雷)[1,2], and Xiaofang Zhao(赵小芳)[1,2,3]

[1] *Xinjiang Key Laboratory of Solid State Physics and Devices, Xinjiang University, Urumqi* 830017, *China*
[2] *School of Physical Science and Technology, Xinjiang University, Urumqi* 830017, *China*
[3] *Tarim University, Alar* 843300, *China*

(Received 9 March 2025; revised manuscript received 30 April 2025; accepted manuscript online 7 May 2025)

The H_2 was excited to the H_2 $X^1\Sigma_g^+$ ($v = 1$, $J = 7$) energy level by the stimulated Raman pumping (SRP) technique, and the process of energy redistribution between $H_2(1,7)$ molecule and LiH was studied. The particle population density of $H_2(1,7)$ energy level is obtained by the coherent anti-Stokes Raman scattering (CARS) technique. The particle population density of each rotational level of H_2 ($v = 1$, $J = 7$, 5, 3) is analyzed with temperature after the collision between $H_2(1,7)$ molecule and LiH. It is found that the particle population density of each level increases with the increase in temperature after the collision. The time-resolved CARS spectra of each rotational energy level of H_2 ($v = 1$, $J = 7$, 5, 3) are analyzed at different temperatures. It is found that a multi-quantum relaxation process with $\Delta J = 4$ occurs in $H_2(1,7)$ molecule, and the temperature accelerates the relaxation process. The effective lifetime of $H_2(1,7)$ energy level is obtained by plotting the semi-logarithmic plots of the CARS signal intensity and delay time of the level, and observing the law of the effective lifetime change with the temperature. It is found that the effective lifetime of $H_2(1,7)$ energy level shows an obvious decreasing trend with the increase of temperature.

Keywords: coherent anti-Stokes Raman scattering, particle population density, multiple quantum relaxation, effective lifetime

PACS: 34.50.–s, 34.20.–b

DOI: 10.1088/1674-1056/add502 **CSTR:** 32038.14.CPB.add502

1. Introduction

Diatomic molecular collision energy transfer is a key research topic in the field of physical chemistry, involving molecular energy transfer, collision dynamics, and intermolecular interactions.[1–5] When a molecule in the vibrationally excited state collides with other molecules, the collision energy may lead to changes in the vibrational, rotational, and translational states of the molecule. This in turn affects the distribution of energy within the molecule.[6,7] In modern scientific progress, collisional energy transfer has been widely used in the fields of the atmospheric environment, the astrophysics, and the dynamics of chemical reactions,[8–14] for example, in interstellar space, inelastic collisional energy transfer between molecules is the main mechanism of interstellar gas cooling.[15,16] When high-energy molecules collide inelastically with low-temperature molecules, some of the internal energy of the high-energy molecules (e.g., vibrational or rotational energy) can be transferred to the low-temperature molecules, causing the energy of the high-energy molecules to decrease, thus realizing the cooling of the gas. Scientists can observe the process of energy redistribution in intermolecular collisions using laser technology, spectroscopic methods and other high-resolution techniques, and study the law of energy redistribution in the process of molecular collisions under different conditions. Over the years, research on energy transfer in intermolecular collisions has progressed, especially with the breakthroughs in technologies such as ultraviolet pulsing,[17,18] overtone pumping,[19] stimulated-emission pumping,[20] and pulsed-laser photo-dissociation.[21] These technologies provide a broad research base for in-depth discussion of the phenomenon of energy transfer between molecules in highly vibrational excited states.

Many experiments and theories have been devoted to the studying model temperatures,[22,23] collisional transfer cross sections,[24] collisional energy transfer rate coefficients,[25,26] charge transfer cross section,[27] quantum relaxation,[28,29] and energy transfer probability distributions[30] for excited state molecules, etc. Wang *et al.*[31] studied the collision process between a highly vibrational excited state, KH ($v'' = 14$–23), and H_2 and N_2, and found that the vibrational energy transfer rate coefficients increase linearly with the vibrational quantum population. In KH($v'' = 20$) + H_2 collisions, the two-qubit energy transfer process ($\Delta v = 2$) plays an important role. In KH($v'' = 20$) + N_2 collisions, the five-qubit energy transfer

[†]These authors contributed equally to this work.
[‡]Corresponding author. E-mail: wsysmilerr@sina.com

© 2025 Chinese Physical Society and IOP Publishing Ltd. All rights, including for text and data mining, AI training, and similar technologies, are reserved.

process ($\Delta v = 5$) also plays a non-negligible role. In addition, the mass effect has a significant influence on the energy transfer rate coefficient, while the vibrational–rotational energy transfer mechanism plays a dominant role in the energy transfer process of the KH molecule. Shen *et al.*[32] investigated the collisional energy transfer process between $H_2(E)$ and LiH, and measured the complete state-resolved distributions of the scattered LiH molecules after excitation of $H_2(E)$ by stimulated Raman pumping. It was found that the translational kinetic energy and rotation distribution of the scattered LiH molecules are very sensitive to the energy of $H_2(E)$, and the rotation distribution is characterized by a biexponential distribution. In addition, V–RT (vibrational–rotational translational) energy transfer is the main energy transfer channel between LiH and $H_2(E)$. Kabir *et al.*[33] confirmed the excitation of the vibrational–rotational energy level of HBr(v, J) using the CARS signal, and measured the total removal rate constants and the state-to-state rate constants of the different rotational energy levels of the collision of HBr($v = 1$, J) and HBr molecules. The results show that the rotational energy transfer (RET) rate constants are much larger than the hard sphere collision rate constants and decrease with increasing initial energy level J. The RET rate constants are much larger than the hard sphere collision rate constants. The $J = 1$ transfer process is found to be the most common, but the multi-quantum transfer process is also found to play an important role. By comparing the experimental data with various rate constant models, it is found that the statistical power-exponential gap law best represents the RET properties of HBr molecular collisions.

There have been many studies on the energy transfer process between excited alkali metal hydrides and gas molecules.[34,35] However, there are relatively few studies on the energy transfer process during collisions between excited state molecules and ground state alkali metal hydrides, especially for the excited state molecules after the collision. For this reason, we have carried out an experimental study of the collisional energy transfer between excited state H_2 and LiH molecules at different temperatures. Because of the large gap between neighboring vibrational energy levels (about 4000 cm^{-1}) in the ground electronic state of H_2, only the lower vibrational states of H_2 can be excited. Collisional transfer between vibrational states is not easy to occur. Because H_2 is a homonuclear diatomic molecule, there is no infrared spectral emission or absorption between vibrational energy levels in the same electronic state, so it cannot be detected using infrared emission or infrared absorption spectroscopy, and because the H_2 ground state is very far away from the first electronic excited state, such as $H_2(X^1\Sigma_g^+\ v = 1)$ and $H_2(B^1\Sigma_g^+\ v = 1)$ states are separated by 10.6 eV, which corresponds to 117-nm[36] wavelength, so it also cannot be detected by laser induction fluorescence spectroscopy, therefore, we utilize the CARS technique to probe the distribution of each vibrational–rotational energy level of H_2.

In this study, the H_2 is excited to the H_2 $X^1\Sigma_g^+$ ($v = 1$, $J = 7$) energy level by the SRP technique, followed by collisional energy transfer with the LiH $X^1\Sigma_g^+$ ($v'' = 0$) molecule. The partial collision energy transfer process in the heat pipe oven is as follows:

$$\begin{aligned} &H_2(1,7) + \mathrm{LiH}(0,3) \\ &\rightarrow H_2(1,5) + \mathrm{LiH}(0,13) + 203.66\ \mathrm{cm}^{-1}, \qquad (1) \\ &H_2(1,7) + \mathrm{LiH}(0,4) \\ &\rightarrow H_2(1,3) + \mathrm{LiH}(1,12) + 142.16\ \mathrm{cm}^{-1}, \qquad (2) \\ &H_2(1,7) + H_2(0,7) \\ &\rightarrow H_2(1,3) + H_2(1,5) - 48.88\ \mathrm{cm}^{-1}. \qquad (3) \end{aligned}$$

Using the CARS detection technique, the CARS signals of each vibrational energy level of H_2 are probed separately. The particle population density, the relaxation process, and the effective lifetime between the vibrational energy levels are measured, as well as their dependence on temperature.

2. Experimental methods

The experimental setup is shown in Fig. 1, and the sample cell is a five-arm crossed heat pipe oven, in which four arms are crossed in a plane, the longer left and right arms are used for laser injection and detection, and the fifth arm is perpendicular to this plane, and its bottom is put into Li metal, which is heated by an electric heater, and the sample cell temperature is measured by a thermocouple. The heat pipe oven was connected to a vacuum and gas injection system. The vacuum in the heat pipe oven was controlled to 10^{-3} Pa before filling with gas, and then 1.3×10^3 Pa (with an error of ± 5 Pa) of H_2 was filled. It was heated utilizing an electric heating unit with the initial temperature set at 680 ± 1 K and the vapor pressure of Li atoms at 1 Pa–1.3 Pa.[37] A fiber optic probe (200 nm–1100 nm detection segment) of the ICCD was placed at the end of the window through which the laser of the heat pipe oven passed and was used to detect the CARS signal.

A dye laser (model: ATM200, LTB laser technology) pumped by an N_2 laser (model: MNL 205-C, LTB laser technology) was tuned to 670.9 nm to excite the Li(2S) ground state energy level to the Li(2P) excited state energy level. Li(2P) will subsequently react with H_2 to form LiH $X^1\Sigma_g^+$ ($v'' = 0$). An intense fluorescence signal at 670.9 nm was detected for Li (2P–2S), confirming that Li(2P) is indeed excited by a dye laser. Acquisition of $H_2(1,7)$ energy level by SRP technique: a 532-nm laser from a YAG laser and a 775.1-nm laser from an OPO (optical parametric oscillator) jointly excited the ground state $H_2(0, 5)$ to the excited state $H_2(1, 7)$

($\Delta E = 5500\ \mathrm{cm}^1$). Both laser beams were vertically polarized, and a lens was used to focus the Raman excitation beam to the center of the sample cell. The time delay (t_D) between the dye laser pulse and the YAG laser pulse was controlled by the DG535 so that the YAG–OPO pulsed laser shot was 10-ns later than the dye laser shot, ensuring that Li(2P) reacted with H_2 to produce LiH.

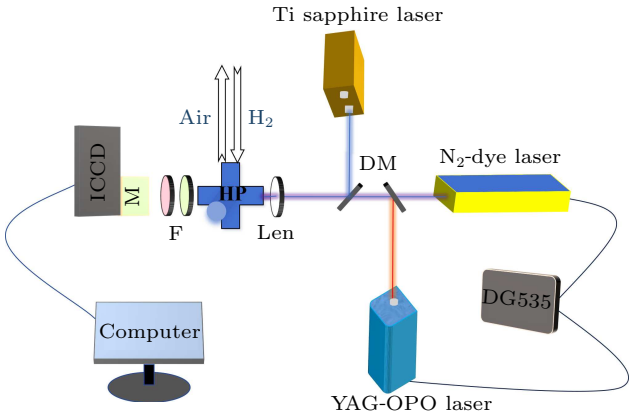


Fig. 1. Diagram of the experimental setup, ICCD: intensified charge-coupled device, M: monochromator, F: filter, HP: heat pipe oven, Len: lens, DM: dichroic mirror, OPO: optical parametric oscillator; DG535: delay generator.

Figure 2 shows the pump detection process of H_2, where a filter capable of filtering both YAG and OPO laser beams is placed between the fiber probe and the left window end of the heat pipe oven. This protects the fiber probe from damage by strong lasers and avoids the interference of the laser wavelengths on the detection signals. Figure 3 shows the scanned CARS spectrum of the S(4) branch of the 1–0 vibrational band of H_2. A peak in the CARS spectrum is observed at $5530 \pm 10\ \mathrm{cm}^{-1}$, which can prove that $H_2(1, 7)$ energy level is successfully excited.

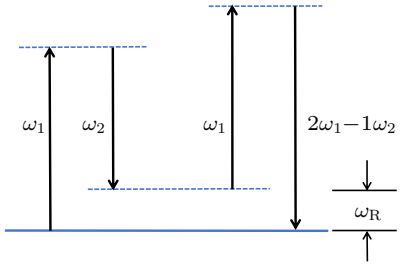


Fig. 2. $H_2(0, 5) \rightarrow H_2(1, 7)$ energy level pump-detect energy level diagram, ω_1: pump light frequency, ω_2: probe light frequency, $2\omega_1 - 1\omega_2$: frequency corresponding to the CARS signal.

After the excitation of H_2 ($v = 0$) to $H_2(1,7)$ energy level using SRP technique, the 532-nm wavelength of laser light emitted from the YAG laser is used as the pump light ω_1 and the 755.1-nm wavelength of laser light emitted from the Ti gemstone laser is used as the probe light ω_2. The collision of $H_2(1,7)$ energy level with LiH molecules occurs with an energy transfer, which makes H_2 obtain different rotational states. Keeping the 532-nm laser light emitted by the YAG laser unchanged, the laser output wavelength of the Ti sapphire laser was adjusted to 716.3 nm, 735.8 nm, and 755.1 nm (corresponding to the three energy levels of $H_2(1,3)$, $H_2(1,5)$, and $H_2(1,7)$, respectively) in turn, as the probe light ω_2 for the CARS spectrum, and the ICCD was again used for CARS signal detection.

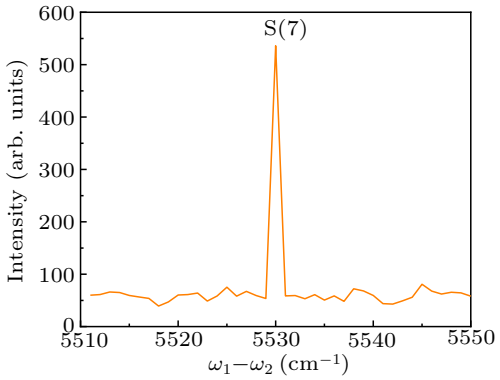


Fig. 3. Scanning CARS spectra of the S(7) branch of the 1–0 vibrational band of H_2($\omega_1 = 532$ nm, $\omega_2 = 775.1$ nm). Intensity is the spectral intensity, and ω_1–ω_2 are the frequency differences between H_2 (0, 5) and H_2(1, 7) energy levels.

3. Results and analysis

3.1. Scanning CARS spectrum of H_2

When H_2 was successfully excited, the scanned CARS signals of $H_2(0,7)$ and $H_2(1,7)$ energy levels were detected, respectively, and figure 4 shows the scanned CARS spectra of $H_2(0,7)$ and $H_2(1,7)$ energy levels.

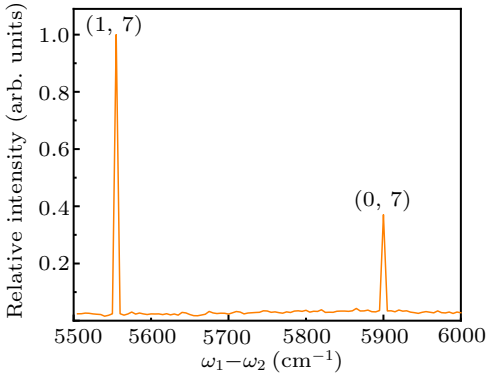


Fig. 4. Scanning CARS spectra of $H_2(0,7)$ and $H_2(1,7)$ energy levels at $T = 680$ K. Relative intensity is the relative spectral intensity, i.e., the spectral intensities are normalized so that the intensity differences between the different energy levels can be compared more easily. $\omega_1 = 532$ nm and $\omega_2 = 764.6$ nm for $H_2(0,7)$ energy level; $\omega_1 = 532$ nm and $\omega_2 = 755.1$ nm for the $H_2(1,7)$ energy level.

The CARS signal strength can be expressed as

$$I \propto (\Delta n)^2 I_{\mathrm{pump}}^2 I_{\mathrm{probe}}, \tag{4}$$

where I is the intensity of the corresponding CARS signal, I_{pump} and I_{probe} are the intensities of the pump light (532 nm) and the probe light (depending on the energy level) in the experiment, respectively, and Δn is the population difference between the two Raman resonance energy levels. The intensity of the light in this experiment I_{pump} is constant, and the wavelength of the probe light changes accordingly with the change of H_2 energy level, and the intensities of the CARS signals

I_0, I_1, I_2, and I_3 at $H_2(0,7)$, $H_2(1,3)$, $H_2(1,5)$, and $H_2(1,7)$ energy levels can be written as

$$I_0 \propto (n_0-n_1)^2 I_{\text{pump}}^2 I_{\text{probe0}}, \tag{5}$$

$$I_1 \propto (n_1-n_2)^2 I_{\text{pump}}^2 I_{\text{probe1}}, \tag{6}$$

$$I_2 \propto (n_2-n_3)^2 I_{\text{pump}}^2 I_{\text{probe2}}, \tag{7}$$

$$I_3 \propto (n_3-n_4)^2 I_{\text{pump}}^2 I_{\text{probe3}}. \tag{8}$$

Since particle populations are not detected at $H_2(1, 9)$, $H_2(2, 5)$, $H_2(2, 7)$, and $H_2(2, 9)$ energy levels, equations (5)–(8) can be simplified as follows:

$$I_0 \propto n_0^2 I_{\text{pump}}^2 I_{\text{probe0}}, \tag{9}$$

$$I_1 \propto n_1^2 I_{\text{pump}}^2 I_{\text{probe1}}, \tag{10}$$

$$I_2 \propto n_2^2 I_{\text{pump}}^2 I_{\text{probe2}}, \tag{11}$$

$$I_3 \propto n_3^2 I_{\text{pump}}^2 I_{\text{probe3}}, \tag{12}$$

where n_0, n_1, n_2, and n_3 denote the particle population densities of H_2 molecules on $H_2(0,7)$, $H_2(1,3)$, $H_2(1,5)$, and $H_2(1,7)$ energy levels, respectively. Assuming that the above equations have the same proportionality constants, the corresponding ratios can be obtained from Eqs. (9)–(12):

$$\left(\frac{n_1}{n_0}\right)^2 = \frac{I_1}{I_0}\cdot\frac{I_{\text{probe0}}}{I_{\text{probe1}}}, \tag{13}$$

$$\left(\frac{n_2}{n_1}\right)^2 = \frac{I_2}{I_1}\cdot\frac{I_{\text{probe1}}}{I_{\text{probe2}}}, \tag{14}$$

$$\left(\frac{n_3}{n_2}\right)^2 = \frac{I_3}{I_2}\cdot\frac{I_{\text{probe2}}}{I_{\text{probe3}}}. \tag{15}$$

The wavelength of the detected light is adjusted and its output power is calibrated so that the ratio of the detected light intensity $I_{\text{probe}\,i}/I_{\text{probe}\,j}$ is a constant value. The initial temperature of this experiment is 680 K, and the gas pressure is 1.3×10^3 Pa (the vapor pressure produced by alkali metals is negligible compared to H_2). The equation for the Boltzmann rotation distribution is given below:

$$N_J = N\frac{hcB}{KT}(2J+1)\exp\left[-\frac{BJ(J+1)hc}{KT}\right]. \tag{16}$$

The particle population density of $H_2(0,7)$ energy level can be obtained as $n_{(0,7)} = 2.6\times10^{14}$ cm^{-3}. From Fig. 4, combined with the relationship between the CARS signal intensity ratio and the particle population density ratio, the particle population density of $H_2(1,7)$ energy level at the initial moment (before the collision occurs) can be obtained as $n*_{(1,7)} = (3.25\pm0.13)\times10^{20}$ cm^{-3} (errors are standard deviations).

3.2. Variation of particle population density with temperature

When $H_2(1,7)$ molecule collides with LiH, it causes $H_2(1,3)$ and $H_2(1,5)$ energy levels to produce the distribution. To further investigate the variation of particle population density with temperature after the occurrence of collision, the temperature of the heat pipe oven is adjusted to the range of 680 K–750 K. The temperature gradient is varied as a temperature gradient every 10 K. Scanning CARS detections are performed for $H_2(1,3)$, $H_2(1,5)$, $H_2(1,7)$, and $H_2(0,7)$ energy levels at the 2nd μs after the occurrence of the collision, respectively, as shown in Fig. 5.

The particle population densities of $H_2(1,3)$, $H_2(1,5)$, and $H_2(1,7)$ energy levels at different temperatures can be obtained by deriving the density equation given in Subsection 3.1, as shown in Table 1.

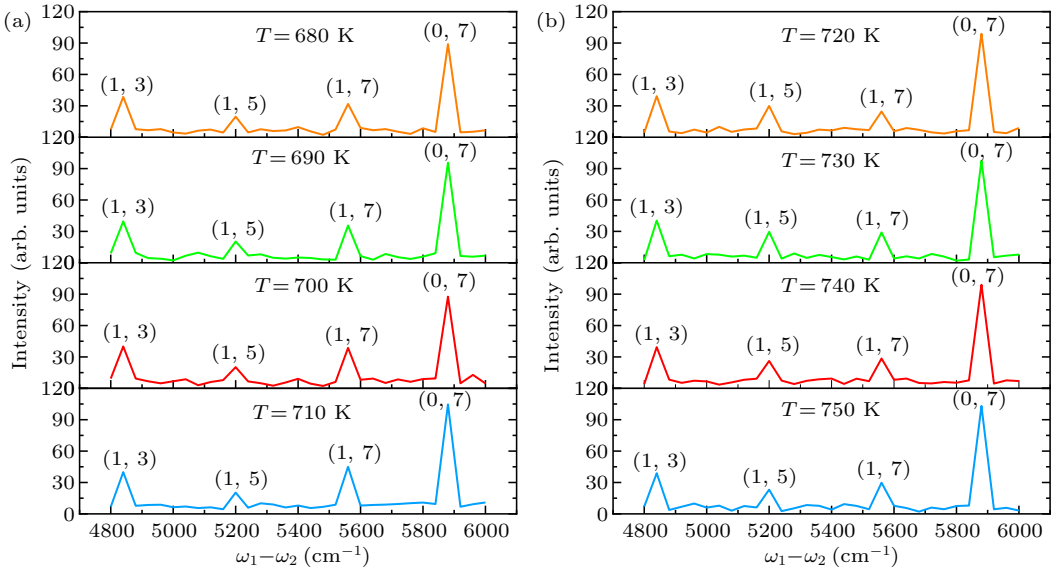


Fig. 5. Partially scanning CARS spectra of $H_2(1,3)$, $H_2(1,5)$, $H_2(1,7)$, and $H_2(0,7)$ energy levels at different temperatures for a delay time of $t_D = 2$ μs. (a) $T = 680$ K–710 K; (b) $T = 720$ K–750 K.

Table 1. Particle population densities of $H_2(1,3)$, $H_2(1,5)$, and $H_2(1,7)$ energy levels at different temperatures at the 2nd μs after the collision of $H_2(1,7)$ molecule with LiH.

Temperature (K)	$n_{(1,3)}$ (10^{20} cm^{-3})	$n_{(1,5)}$ (10^{20} cm^{-3})	$n_{(1,7)}$ (10^{20} cm^{-3})
680	1.22 ± 0.15	0.87 ± 0.11	1.29 ± 0.17
690	1.43 ± 0.12	1.02 ± 0.15	1.42 ± 0.12
700	1.47 ± 0.17	1.05 ± 0.20	1.39 ± 0.19
710	1.61 ± 0.14	1.15 ± 0.22	1.46 ± 0.17
720	1.61 ± 0.13	1.24 ± 0.14	1.41 ± 0.24
730	1.76 ± 0.19	1.44 ± 0.17	1.50 ± 0.12
740	1.92 ± 0.18	1.64 ± 0.25	1.63 ± 0.19
750	2.00 ± 0.13	1.74 ± 0.20	1.58 ± 0.12

As shown in Table 1, at $T = 680$ K, the particle population density of $H_2(1,7)$ energy level decreases to $(1.29\pm0.17)\times10^{20}$ cm^{-3} at the 2nd μs after the collision of $H_2(1,7)$ molecules with LiH. This indicates that the collision process of the first 2 μs decreases the particle population density of $H_2(1,7)$ energy level by 60%. Figure 6 shows the variation of particle population densities of $H_2(1,3)$, $H_2(1,5)$, and $H_2(1,7)$ energy levels at different temperatures.

From Fig. 6, it can be found that the particle population densities of $H_2(1,3)$, $H_2(1,5)$, and $H_2(1,7)$ energy levels tend to increase with increasing temperature. Among them, $H_2(1,3)$ and $H_2(1,5)$ energy levels change over a larger range, while $H_2(1,7)$ energy level changes over a smaller range. This is because the total particle population density in the oven increases due to the increase in temperature, but with the increase in temperature, the average kinetic energy of the molecules increases, and the collisions between the molecules are more frequent and violent. This causes the populations of $H_2(1,7)$ energy levels to decrease more rapidly, so that the changes in $H_2(1,3)$ and $H_2(1,5)$ levels are more pronounced than those in $H_2(1,7)$ energy levels.

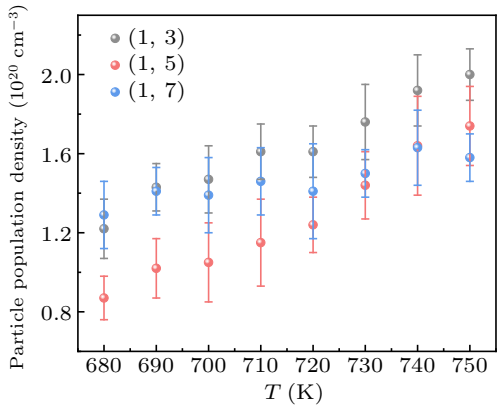


Fig. 6. Variation of particle population densities of $H_2(1,3)$, $H_2(1,5)$, and $H_2(1,7)$ energy levels with temperature in the temperature range of 680 K–750 K at the 2nd μs after the collision of $H_2(1,7)$ molecule with LiH.

3.3. Temperature dependence of the collisional relaxation process

To study the collisional relaxation of $H_2(1,7)$ energy level after the collision of $H_2(1,7)$ molecules with LiH and the effect of temperature on the process, the time delay was set to 8 μs after the collision occurred. Time-resolved CARS curve profiles of $H_2(1,3)$, $H_2(1,5)$, and $H_2(1,7)$ energy levels at different temperatures are measured by varying the temperature in the heat pipe oven in a range of 680 K–750 K with a 10-K gradient.

Figure 7 shows the evolution of the particle populations with time delay for $H_2(1,3)$, $H_2(1,5)$, and $H_2(1,7)$ energy levels at different temperatures.

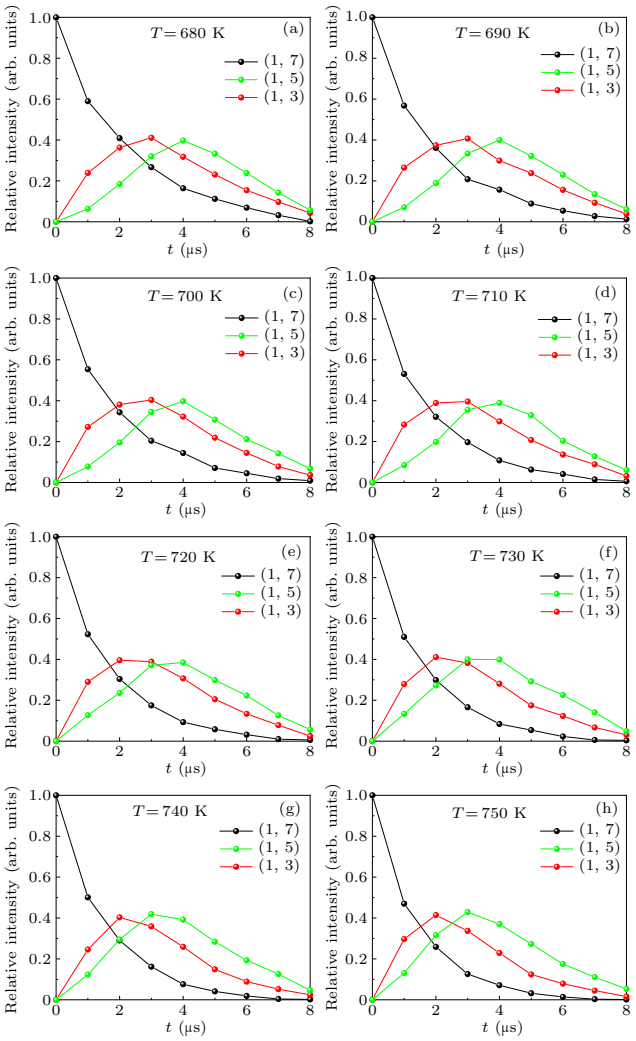


Fig. 7. With a delay time of $t_D = 8$ μs, the evolution curves of the particle populations on $H_2(1,3)$, $H_2(1,5)$, and $H_2(1,7)$ energy levels with delay time are measured within the temperature range of 680 K–750 K: (a) $T = 680$ K, (b) $T = 690$ K, (c) $T = 700$ K, (d) $T = 710$ K, (e) $T = 720$ K, (f) $T = 730$ K, (g) $T = 740$ K, (h) $T = 750$ K.

From Fig. 7, it can be seen that the particle populations of $H_2(1,7)$ energy level decrease rapidly with the collision, while the particle populations of $H_2(1,3)$ and $H_2(1,5)$ energy levels increase gradually, and the particle populations on $H_2(1,3)$ energy level evolves faster than that on $H_2(1,5)$ energy level. This suggests that the multi-quantum relaxation of $\Delta J = 4$ occurs in $H_2(1,7)$ molecule. The relaxation of $H_2(1,3)$ energy level accelerates with increasing temperature. At a cell temperature of 680 K, the particle populations on $H_2(1,3)$ energy level reaches its peak at approximately 2.5 μs. At a cell temperature of 750 K, the particle populations on $H_2(1,3)$ energy level reaches its peak at approximately 2 μs. This indicates that the temperature has a good promotional effect on the relaxation process. When the temperature is increased, the particle in the system obtains more thermal energy, which leads to its more frequent leaps between quantum states, thus accelerating the whole relaxation process. The increase in temperature causes the rotational energy of $H_2(1,7)$ molecule to be transferred to the rotational energy of the LiH molecule more quickly. This indicates that the energy transfer in the hybrid system at this time is dominated by multi-quantum relaxation and that the energy transfer mode is primarily governed by R-R collisional relaxation.

3.4. Effect of temperature on effective lifetime of $H_2(1, 7)$ energy level

The particle population density of $H_2(1,7)$ molecule as a function of time decay can be described approximately as

$$N_J(t) = N_0 \, \mathrm{e}^{-t/\tau}, \tag{17}$$

where $N_J(t)$ denotes the particle population density of $H_2(1,7)$ energy level, τ denotes the effective lifetime of $H_2(1,7)$ energy level, and N_0 is the initial population density of the $H_2(1,7)$ energy level at $t = 0$. Substituting Eq. (4) into Eq. (17), we have

$$I_J(t) \propto I_{\mathrm{pump}}^2 I_{\mathrm{probe}} N_0^2 \, \mathrm{e}^{-2t/\tau} = I_0 \, \mathrm{e}^{-2t/\tau}. \tag{18}$$

Taking logarithms on both sides of Eq. (18), the effective lifetime τ of $H_2(1,7)$ energy level can be obtained from the following equation:

$$\ln\left[I_J(t)/I_0\right] = -2\frac{t}{\tau}. \tag{19}$$

By measuring the evolution profile of the CARS signal intensity of $H_2(1,7)$ energy level with delay time at different temperatures, the semi-logarithmic plots of the variation of the CARS signal intensity and delay time of $H_2(1,7)$ energy level are plotted. The effective lifetimes can be obtained from the slopes of the straight lines. Figure 8 represents the semi-logarithmic of the variation of CARS signal intensity and delay time for $H_2(1,7)$ energy level at different temperatures. The corresponding effective lifetimes are listed in Table 2.

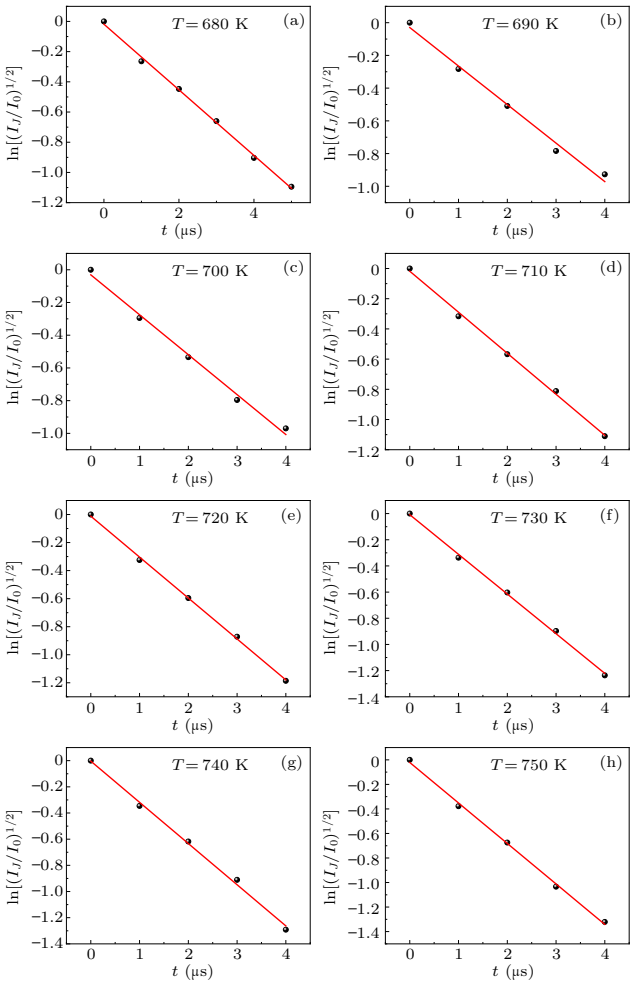


Fig. 8. Semi-logarithmic plots of the variation of CARS signal intensity and delay time for $H_2(1,7)$ energy level in the temperature range of 680 K–750 K. The decay rate of the population obtained from the slope is $1/\tau$: (a) $T = 680$ K, (b) $T = 690$ K, (c) $T = 700$ K, (d) $T = 710$ K, (e) $T = 720$ K, (f) $T = 730$ K, (g) $T = 740$ K, (h) $T = 750$ K.

Table 2. Effective lifetimes of $H_2(1,7)$ energy level in the temperature range of 680 K–750 K (from the slope in Fig. 8).

Temperature (K)	Lifetime τ (μs)	Temperature (K)	Lifetime τ (μs)
680	4.61 ± 0.03	720	3.42 ± 0.06
690	4.26 ± 0.09	730	3.30 ± 0.07
700	4.10 ± 0.10	740	3.18 ± 0.09
710	3.68 ± 0.09	750	3.03 ± 0.07

Figure 9 is plotted according to $H_2(1,7)$ energy level effective lifetime data with temperature in Table 2. It can be seen from Fig. 9 that the effective lifetime of $H_2(1,7)$ energy level shows a clear decreasing trend with increasing temperature. It indicates that the increase in temperature results in an increase in the thermal motion of the molecules, which in turn causes more frequent collisions and thereby increases the frequency of collisions between them. Collisions cause particles to return from the excited state to the ground state, or to transfer from one energy state to another. Therefore, the increase in collision frequency shortens the average residence time of particles in a particular energy state, i.e., it accelerates the quenching of the population in $H_2(1,7)$ energy level, which also advances the quantum relaxation process.

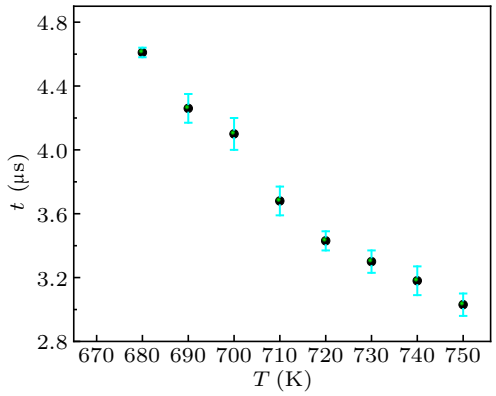


Fig. 9. The variation of the effective lifetime of $H_2(1,7)$ energy level with temperature ranging from 680 K–750 K.

4. Conclusion

In this study, H_2 is excited to the state of $H_2(1,7)$ by SRP technology. After the collision with LiH, the particle populations appear at the energy levels of $H_2(1,3)$, $H_2(1,5)$, and $H_2(1,7)$. Using the scanning CARS technique to detect the particle number density in $H_2(0,7)$ and $H_2(1,7)$ energy levels before the collision. 2 μs after the collision, particle distributions also appear in $H_2(1,3)$ and $H_2(1,5)$ energy levels. The particle number densities in $H_2(1,3)$, $H_2(1,5)$, and $H_2(1,7)$ energy levels are then detected post-collision. Using the time-resolved CARS technique, the evolution of the particle population densities of $H_2(1,3)$, $H_2(1,5)$ and $H_2(1,7)$ energy levels with temperature after the collision is investigated, the collisional relaxation process is analyzed, and the effective lifetimes of $H_2(1,7)$ energy level are obtained for different temperatures utilizing the semi-logarithmic plots of the changes in the CARS signal intensities and delay times of the $H_2(1,7)$ energy level. After the collision of $H_2(1,7)$ molecules with LiH, the particle population density of $H_2(1,7)$ energy level decreases by 60%, with the population transferring to $H_2(1,3)$ and $H_2(1,5)$ energy levels. At 2-μs post-collision, the particle population densities of $H_2(1,3)$, $H_2(1,5)$, and $H_2(1,7)$ energy levels show an increasing trend with rising temperature. The collision causes a rapid decrease in the population of $H_2(1,7)$ energy level particles, while the population of $H_2(1,3)$ energy level particles increases before that of $H_2(1,5)$ energy level particles, confirming the collision to be a multi-quantum relaxation process with $\Delta J = 4$. The effective lifetime of $H_2(1,7)$ energy level exhibits a decreasing trend with increasing temperature.

Acknowledgements

Project supported by the Natural Science Foundation of Xinjiang Uygur Autonomous Region (Grant No. 2023D01C06) and the National Natural Science Foundation of China (Grant No. 12164047).

References

[1] Hong Q Z, Sun Q H, Pirani F, Valentín Rodríguez M A, Hernández Lamoneda R, Coletti C, Hernández M I and Bartolomei M 2021 *J. Chem. Phys.* **154** 064304
[2] Hong Q Z, Bartolomei M, Coletti C, Lombardi A, Sun Q H and Pirani F 2021 *Molecules* **26** 7152
[3] Sun Z F, van Hemert M C, Loreau J, van der Avoird A, Suits A G and Parker D H 2020 *Science* **369** 307
[4] Towski M, Loreau J and Lique F 2022 *Phys. Chem. Chem. Phys.* **24** 11910
[5] Tang G Q, Besemer M, de Jongh T, Shuai Q, van der Avoird A, Groenenboom G C and van de Meerakker S Y T 2020 *J. Chem. Phys.* **153** 064301
[6] Wünderlich D, Scarlett L H, Briefi S, Fantz U, Zammit M C, Fursa D V and Bray I 2021 *J. Phys. D: Appl. Phys.* **54** 115201
[7] Wan Y, Yang B H, Stancil P C, Balakrishnan N, Parekh N J and Forrey R C 2018 *Astrophys. J.* **862** 132
[8] Schiffman A and Chandler D W 1995 *Int. Rev. Phys. Chem.* **14** 371
[9] Ogurtsov G N, Il'In R N, Lavrov V M and Avakyan S V 2000 *Phys. Chem. Earth (C)* **25** 587
[10] Lee R A, Ajello J M, Malone C P, Evans J S, Veibell V, Holsclaw G M, McClintock W E, Hoskins A C, Jain S K and Gérard J C 2022 *Astrophys. J.* **938** 99
[11] Li L, Leys C, Britun N, Snyders R and Nikiforov A Y 2014 *IEEE Trans. Plasma Sci.* **42** 2752
[12] Deng X L, Nikiforov A Y, Ionita E R, Dinescu G and Leys C 2015 *Appl. Phys. Lett.* **107** 053702
[13] Lytras I, Mitsopoulos E P, Dogkas E and Koutmos P 2020 *Combust. Explos. Shock Waves* **56** 278
[14] López-Cámara C F, Saggese C, Pitz W J, Shao X, Im H J and Dunn-Rankin D 2023 *Combust. Flame* **253** 112822
[15] Mandal B, Joy C, Semenov A and Babikov D 2022 *ACS Earth Space Chem.* **6** 521
[16] MTielens A G G 2005 *The physics and chemistry of the interstellar medium* (London: Cambridge University Press) p. 96
[17] Havey D K, Du J, Liu Q N and Mullin A S 2010 *J. Phys. Chem. A* **114** 1569
[18] Du J, Sassin N A, Havey D K, Hsu K and Mullin A S 2013 *J. Phys. Chem. A* **117** 12104
[19] Hartland G V, Qin D and Dai H L 1994 *J. Chem. Phys.* **101** 8554
[20] Jongma R T and Wodtke A M 1999 *J. Chem. Phys.* **111** 10957
[21] Yamasaki K, Fujii H, Watanabe S, Hatano T and Tokue I 2006 *Phys. Chem. Chem. Phys.* **8** 1936
[22] McCaffery A J, Pritchard M, Turner J F C and Marsh R J 2011 *J. Phys. Chem. A* **115** 4169
[23] McCaffery A J 2016 *J. Chem. Phys.* **144** 194304
[24] Yang H W, Liu X Y, Liu Y Q, Xu M H and Li Z 2023 *J. Chem. Phys.* **159** 124306
[25] Michael T J, Ogden H M and Mullin A S 2021 *J. Chem. Phys.* **154** 134307
[26] Hoshino S, Yamamoto O and Tsukiyama K 2022 *ACS Omega* **7** 3605
[27] Zhang H H, Yu W D, Gao C Z and Qu Y Z 2023 *Chin. Phys. Lett.* **40** 043101
[28] Chen G Q, Liu J, Alghazi A and Wang Q 2021 *Russ. J. Phys. Chem. B* **15** 764
[29] Koide N, Haze M, Okuda Y, Yamasaki K and Kohguchi H 2023 *Chem. Phys. Lett.* **833** 140932
[30] Fu Y L and Han Y C 2021 *Chem. Phys. Lett.* **776** 138676
[31] Wang S Y, Zhang B, Zhu D H, Dai K and Shen Y F 2012 *Spectrochim Acta A* **96** 517
[32] Shen X Y, Wang S Y, Dai K and Shen Y F 2017 *Spectrochim Acta A* **173** 516
[33] Kabir H, Antonov I O and Heaven M C 2009 *J. Chem. Phys.* **130** 074305
[34] Liu J, Shen X Y and Dai K 2013 *Chem. Phys.* **425** 62
[35] Alghazi A, Liu J, Dai K and Shen Y F 2015 *Chem. Phys.* **448** 76
[36] Pachucki K and Komasa J 2009 *J. Chem. Phys.* **130** 164113
[37] Chen J J, Hung Y M, Liu D K, Fung H S and Lin K C 2001 *J. Chem. Phys.* **114** 9395